



# Steady-state axial profiles of dissolved oxygen in tall bubble column bioreactors

Fernando Camacho Rubio<sup>a</sup>, Jose Luis Garcia<sup>b</sup>, Emilio Molina<sup>b</sup>, Yusuf Chisti<sup>b,\*</sup>

<sup>a</sup> *Department of Chemical Engineering, University of Granada, E-18071 Granada, Spain*

<sup>b</sup> *Department of Chemical Engineering, University of Almería, E-04071 Almería, Spain*

Received 8 May 1998; received in revised form 4 November 1998; accepted 5 December 1998

## Abstract

A model is developed for prediction and interpretation of the observed steady-state axial dissolved oxygen concentration profiles in tall bubble columns. The observed concentration profiles are non-linear, unlike what would be expected if the hydrostatic pressure alone influenced the profiles. The non-linear profiles result from the axial mixing of liquid in the column. Several other factors influence the profiles, including the overall gas holdup, the volumetric overall gas–liquid mass transfer coefficient, and the static height of liquid in the column. The effect of mixing can be adequately accounted for using an axial dispersion coefficient. Because the axial dispersion coefficient is sensitive to the diameter of the column and to gas flow rate, the overall behavior of the profile is affected by the aspect ratio of the column and the superficial gas velocity in it. The mass transfer coefficient and the axial dispersion coefficient have mutually opposing effects on the shape of the profile. Because both those variables increase with increasing gas flow rate, the shape of the profile is affected less than would be the case if only mixing influenced the profile. The non-linearity of concentration profiles increases with increasing overall height of the column especially when the height exceeds about 2 m in a 0.24 m diameter column. The model-predicted axial concentration profiles agree closely – within  $\pm 3\%$  – with the measured data. Using the measured profile, the model allows for calculation of the liquid-phase axial dispersion coefficients. This method does not require the use of tracers. Being a steady-state method, the operation of the bioreactor does not need to be interrupted in any way for the determination of the axial dispersion coefficient or the state of mixing. Consequently, the proposed method is particularly suited to characterizing the axial dispersion coefficient in an operating bioreactor without disturbing the operation. If the axial dispersion coefficient is known, the model allows for quantifying the spatial inhomogeneities in oxygen concentration in a bioreactor vessel. © 1999 Elsevier Science Ltd. All rights reserved.

**Keywords:** Bubble columns; Airlift bioreactors; Oxygen transfer; Axial dispersion; Hydrodynamics

## 1. Introduction

Bubble columns and airlift bioreactors are widely used in the bioprocess industry. Typically, the aspect ratio of these devices exceeds four; much greater aspect ratios are the norm for airlift reactors that are employed in biological treatment of wastewater (Chisti, 1989, 1998). The reactors are sparged with air which provides the oxygen needed by the microorganisms. Under steady-state operation, spatial inhomogeneities in dissolved oxygen concentration have been observed in tall bubble columns and airlift vessels (Chisti, 1989, 1998; Russell et al., 1995;

Pollard et al., 1994). The inhomogeneities are particularly pronounced in the axial direction. Variations in dissolved oxygen concentration potentially affect the local and the overall productivity of bioreactors; hence, quantification of axial changes in concentration is necessary. This paper develops a model for predicting the nature of the steady-state axial profiles of dissolved oxygen in bubble columns. The model is demonstrated using data measured in tall bioreactors (aspect ratio  $\sim 16.5$ ). The profiles are shown to be sensitive to several factors, including the overall volumetric gas–liquid mass transfer coefficient, the liquid-phase axial dispersion coefficient, and other geometric, hydrodynamic, and operational characteristics of the reactors. The developed model provides a predictive and interpretive capability for the observed axial variation of dissolved oxygen in bubble columns.

\* Corresponding author. Tel.: + 34-950-21-5566; fax: + 34-950-21-5484; e-mail: ychisti@ualm.es.

## 2. Theory

In a bubble column with a gas–liquid dispersion height  $h_D$ , the hydrostatic pressure at any axial location  $z$  from the bottom of the column can be shown to be

$$P(z) = P_a + \rho_L(1 - \varepsilon_G)g(h_D - z), \quad (1)$$

where  $P_a$  is the pressure in the headspace of the column,  $\rho_L$  is the density of the liquid,  $g$  is the gravitational acceleration, and  $\varepsilon_G$ , the gas holdup, is assumed to be axially invariant (Reith et al., 1968). As is the usual case, the solubility of a sparingly soluble gas such as oxygen is governed by Henry's law; hence, the saturation concentration ( $C_0^*$ ) of dissolved oxygen at any axial position  $z$  is given by the equation

$$C_0^* = \frac{y_0 P(z)}{H_0} = \frac{y_0 P_a + y_0 \rho_L(1 - \varepsilon_G)g(h_D - z)}{H_0}, \quad (2)$$

where  $y_0$  and  $H_0$  are the mole fraction of oxygen in the gas-phase and the Henry's law constant, respectively. Eq. (2) assumes a constant gas-phase composition which is generally valid in view of the short residence time of gas in the column (Chisti, 1989). As shown later in this work, at steady-state, the maximum axial variation in the gas-phase composition is 10% or less in the absence of an oxygen consuming reaction which is the case of interest in this work. Eq. (2) suggests a declining steady-state dissolved oxygen concentration as we move up the column. The axial concentration profile provided by the theoretical equation (2) applies to a hypothetical column with zero axial mixing. Real columns experience a level of axial mixing of liquid which is promoted by movement of gas bubbles relative to the liquid (Shah et al., 1982; Heijnen and Van't Riet, 1984; Ohki and Inoue, 1970; Deckwer et al., 1974; Joshi, 1980; Reith et al., 1968). This axial mixing is expected to reduce the variation in the actual steady-state liquid-phase concentration of oxygen along the column, i.e., the slope of the  $C_0$  vs  $z$  plot should decline with increased axial mixing. Significantly less pronounced axial dissolved oxygen profiles have indeed been reported: in bubble columns and airlift devices having working aspect ratios up to about 21 and gas–liquid dispersion heights up to about 5.6 m, Chisti (1989) recorded substantially lower variations in steady-state axial dissolved oxygen concentrations than expected from Eq. (2). Chisti's observations spanned a variety of fluids, including non-newtonian fibrous slurries, and extremes of mixing situations represented by a broad range of gas flow rates (Chisti, 1989). As detailed here, the altered shape of dissolved oxygen profiles relative to predictions of Eq. (2) provides an elegant, tracer-less method for characterizing the mixing and other parameters in bubble columns and airlift reactors.

Following well established approaches (Shah et al., 1982; Chisti, 1989; Ohki and Inoue, 1970; Deckwer et al.,

1974; Joshi, 1980; Baird and Rice, 1975), the extent of axial mixing in bubble columns can be specified in terms of an axial dispersion coefficient  $D_z$ , and an oxygen mass balance can be written for a control volume made up of a thin horizontal segment of the column having a segment height  $dz$ . The appropriate balance equation is

$$D_z \frac{d^2 C_0}{dz^2} + k_L a_L (C_0^* - C_0) - R = 0. \quad (3)$$

The first term in Eq. (3) represents the change in the dissolved oxygen concentration in the control volume due to axial dispersion; the second term represents the change in concentration due to gas–liquid mass transfer. The mass transfer term consists of a mass transfer coefficient ( $k_L$ ), the specific gas–liquid interfacial area ( $a_L$ ), and a concentration difference driving force ( $C_0^* - C_0$ ). The volumetric rate of possible oxygen consumption is represented as  $R$ , but for the purpose of this work  $R = 0$  and it is disregarded. At steady state there is no net accumulation or depletion of oxygen in the control volume.

Eq. (3) can be made dimensionless using a dimensionless dissolved oxygen concentration  $C$  and a dimensionless height  $x$ , defined respectively as follows:

$$C = \frac{C_0}{y_0 P_b / H_0} \quad \text{and} \quad x = \frac{z}{h_D}, \quad (4)$$

where  $P_b$  is the hydrostatic pressure at the bottom of the column. The dimensionless form of Eq. (3) is

$$\frac{D_z}{h_D^2} \frac{d^2 C}{dx^2} + k_L a_L (C^* - C) = 0, \quad (5)$$

where the dimensionless saturation concentration ( $C^*$ ) of dissolved oxygen at any axial position  $z$  is given as

$$C^* = \psi + \frac{\rho_L(1 - \varepsilon_G)g(h_D - z)}{P_b} = \psi + \alpha(1 - x). \quad (6)$$

The hydrostatic pressure ( $P_b$ ) at the bottom of the column is calculated using Eq. (1) at  $z = 0$ . The parameters  $\alpha$  and  $\psi$  in the above equation are:

$$\alpha = \frac{\rho_L(1 - \varepsilon_G)g h_D}{P_b} = \frac{\rho_L g h_L}{P_b} \quad (7)$$

and

$$\psi = \frac{P_a}{P_b}, \quad (8)$$

respectively. In Eq. (7),  $h_L$  is the height of gas-free liquid; hence, the parameter  $\alpha$  is independent of the gas holdup, although the dimensionless height coordinate has this dependence:

$$x = \frac{z}{h_D} = \frac{z(1 - \varepsilon_G)}{h_L}. \quad (9)$$

Use of expression (6) in Eq. (5) leads to

$$\frac{d^2C}{dx^2} - \beta^2 C = -\beta^2(\psi + \alpha(1 - x)), \quad (10)$$

where the dimensionless parameter  $\beta$  is given as

$$\beta^2 = \frac{k_L a_L h_D^2}{D_z}. \quad (11)$$

The general solution of Eq. (10) is

$$C = cte_1 \exp(\beta x) + cte_2 \exp(-\beta x) + \psi + \alpha(1 - x), \quad (12)$$

where  $cte_1$  and  $cte_2$  are constants of integration.

At steady state, there is no net oxygen transfer between the phases because there is no consumption of oxygen in the liquid. Thus, oxygen transfer from the gas to the liquid in an arbitrary bottom zone of the column needs to balance the transfer in the reverse direction in an arbitrary upper zone. Consequently, at some axial location  $x_C$  the direction of transfer changes. At position  $x_C$ , the concentration of dissolved oxygen in the liquid equals the saturation concentration given by Eq. (2); hence,

$$x = x_C \Rightarrow C = C^* = \psi + \alpha(1 - x_C). \quad (13)$$

Thus,

$$0 = cte_1 \exp(\beta x_C) + cte_2 \exp(-\beta x_C) \quad (14)$$

and

$$cte_2 = -cte_1 \exp(\beta 2x_C). \quad (15)$$

Using this expression in Eq. (12), we obtain

$$C = cte_1 \{ \exp(\beta x) - \exp(\beta(2x_C - x)) \} + \psi + \alpha(1 - x). \quad (16)$$

As pointed out previously, the null net oxygen transfer leads to:

$$\int_0^{h_D} k_L a_L (C_0^* - C_0) S dz = \frac{y_0 P_b S h_D}{H_0} \int_0^1 k_L a_L (C^* - C) dx = 0, \quad (17)$$

where  $S$  is the cross-sectional area of the bubble column. Assuming that the volumetric mass transfer coefficient  $k_L a_L$  is constant, Eqs. (16) and (17) allow for calculation of the axial location  $x_C$  at which the direction of mass transfer reverses; thus,

$$\int_0^1 (C^* - C) dx = 0, \quad (18)$$

or

$$\int_0^1 \{ \exp(\beta x) - \exp(\beta(2x_C - x)) \} dx = 0; \quad (19)$$

therefore,

$$x_C = \frac{1}{2\beta} \ln \left( \frac{\exp(\beta) - 1}{1 - \exp(-\beta)} \right). \quad (20)$$

Eq. (20) gives  $x_C$  as 0.5, irrespective of the  $\beta$  value. This result is intuitively logical, although in practice, specifying  $k_L a_L$  as an axially invariant parameter is an approximation (Deckwer et al., 1978). Conceivably, therefore, the actual  $x_C$  value may be different than 0.5. Nevertheless, for  $x_C = 0.5$  and the boundary condition that at  $x = 0$ ,  $dC/dx = 0$ , the general solution of the mass balance becomes fully defined, with

$$cte_1 = \frac{\alpha}{\beta + \beta \exp \beta} \quad (21)$$

and

$$C = \frac{\alpha \{ \exp(\beta x) - \exp(\beta(2x_C - x)) \}}{\beta + \beta \exp \beta} + \psi + \alpha(1 - x). \quad (22)$$

Two extreme situations can be envisaged with regard to Eq. (22):

- (i) if the axial dispersion coefficient is much greater than the mass transfer coefficient,  $\beta$  tends to zero, and Eq. (22) reduces to

$$C = \psi + 0.5\alpha, \quad (23)$$

that is, the liquid phase is saturated with respect to its average position;

- (ii) when the volumetric gas–liquid mass transfer coefficient is much greater than the liquid-phase axial dispersion coefficient,  $\beta$  tends to infinity, and Eq. (22) becomes

$$C = \psi + \alpha(1 - x). \quad (24)$$

Eq. (24) implies that the liquid phase is saturated at any axial location.

That Eq. (23) is a limiting case of Eq. (22) is not so obvious: limit of the first term on the right-hand side of Eq. (22) is indeterminate as  $\beta$  tends to zero, i.e.,

$$\lim_{\beta \rightarrow 0} \frac{\alpha \{ \exp(\beta x) - \exp(\beta(2x_C - x)) \}}{\beta + \beta \exp \beta} = \frac{\alpha \{ 1 - 1 \}}{0} = \frac{0}{0}. \quad (25)$$

This indeterminate situation is resolved by applying L'Hôpital's rule; thus,

$$\begin{aligned} \lim_{\beta \rightarrow 0} \frac{\alpha \{ x \exp(\beta x) - (2x_C - x) \exp(\beta(2x_C - x)) \}}{\beta + \exp \beta + \beta \exp \beta} \\ = \frac{\alpha \{ x - 2x_C + x \}}{1 + 1} = \alpha(x - x_C). \end{aligned} \quad (26)$$

Substitution of Eq. (26) into Eq. (22) for  $x_C = 0.5$  leads to Eq. (23).

The above analysis disregards any oxygen transfer at the free surface of dispersion at the top of the column. This ‘end effect’ is discussed below.

### 2.1. Influence of the end effect

To account for oxygen transfer across the free surface of dispersion at the head of the column, Eq. (17) may be rewritten as

$$\int_0^{h_D} k_L a_L (C_0^* - C_0) S dz + k_L A_L \left( \frac{y_0 P_a}{H_0} - (C_0)_{x=1} \right) = 0, \quad (27)$$

where  $k_L A_L$  is the total mass transfer coefficient ( $\text{m}^3 \text{s}^{-1}$ ) for oxygen transfer at the free surface. In dimensionless form, Eq. (27) is

$$\frac{y_0 P_b S h_D k_L a_L}{H_0} \left\{ \int_0^1 (C^* - C) dx + \frac{k_L A_L}{S h_D k_L a_L} (\psi - (C)_{x=1}) \right\} = 0, \quad (28)$$

which may be written as

$$\int_0^1 (C^* - C) dx + \phi (\psi - (C)_{x=1}) = 0, \quad (29)$$

where the parameter  $\phi$  is defined as

$$\phi = \frac{k_L A_L}{S h_D k_L a_L}. \quad (30)$$

Substitution of Eq. (29) into Eq. (16) followed by rearrangement yields

$$x_C = \frac{1}{2\beta} \ln \left( \frac{\exp(\beta)(\phi\beta + 1) - 1}{\exp(-\beta)(\phi\beta - 1) + 1} \right). \quad (31)$$

In Eq. (31), when  $\phi$  tends to infinity  $x_C = 1$ , and when  $\phi$  tends to zero  $x_C$  becomes 0.5, i.e.,  $0.5 < x_C < 1$ . Because of this behavior a mass transfer inversion point (i.e.,  $x_C$ ) may be difficult to observe if the influence of the end effect is significant and  $x_C$  is displaced to the top of the column.

Because the  $k_L$  values at the free surface and for the bubbles may be considered approximately equal, and the area  $A_L$  of the free surface is nearly the same as that of the cross-section of the column (i.e.,  $A_L \approx S$ ), the parameter  $\phi$  may be approximated as

$$\phi \approx \frac{1 - \varepsilon_G}{h_L a_L}. \quad (32)$$

Now, the axial oxygen profile including the end effect is given by

$$C = \frac{\alpha \{ \exp(\beta x) - \exp(\beta(2x_C - x)) \}}{\beta + \beta \exp(2\beta x_C)} + \psi + \alpha(1 - x). \quad (33)$$

### 3. Measurements

The bubble column used had a gas-free liquid height of 3.995 m and an overall height of 8.05 m; its diameter was 0.243 m (Chisti, 1989). Potable tap water at 22.8°C was the liquid phase; it had 325  $\text{mg l}^{-1}$  total dissolved solids and a total hardness of 320  $\text{mg l}^{-1}$  (Chisti, 1989). The column was sparged with air through a perforated plate sparger located at the base of the column. The sparger had 106 holes of  $1.0 \times 10^{-3}$  m diameter arranged in a 0.02 m triangular pitch. The free area of the sparger was 0.18% of the cross-sectional area of the column. The column was open to atmosphere and the local atmospheric pressure was 99.5 kPa absolute. The gas was sparged at superficial velocities of  $2.70 \times 10^{-2} \text{ m s}^{-1}$  and  $7.72 \times 10^{-2} \text{ m s}^{-1}$  (Chisti, 1989).

The steady-state dissolved oxygen concentrations were measured at the centerline of the column. The concentration data were reproducible to within  $\pm 3\%$ . The measurements were automatically corrected for temperature variations which remained within  $\pm 2^\circ\text{C}$ . Because the column used was fairly tall, the oxygen electrode had to measure under significantly different hydrostatic pressures. The geometry of the thin polymer membrane at the measuring surface of the electrode can be sensitive to the surrounding pressure (Chisti, 1989); hence, the requirement of a constant membrane geometry (Krebs and Haddad, 1972; Chisti, 1989) for a constant diffusion path to the electrode can be difficult to meet. To prevent geometric distortion, the electrode used was pressure compensated, such that the pressure on either side of the membrane was always the same irrespective of the surrounding pressure (Chisti, 1989). The overall volumetric gas-liquid mass transfer coefficient was determined by the dynamic gassing-in method as explained elsewhere (Chisti, 1989). The overall gas holdup was measured by the volume expansion technique (Chisti, 1989).

### 4. Results and discussion

Eq. (33) was used to fit the model concentration profile to the measured data; two adjustable parameters  $\beta$  and  $x_C$  were used for the fitting with the constraint that  $0.5 < x_C \leq 1.0$ . Furthermore, the  $k_L a_L$  and the height of dispersion in the best-fit  $\beta$  values had to agree exactly with the equations:

$$k_L a_L = 2.39 \times 10^{-4} \left( \frac{P_G}{V_L} \right)^{0.86} \quad (34)$$

and

$$h_D = \frac{h_L}{1 - \varepsilon_G}, \quad (35)$$

where  $h_L$  was 3.995 m. The gas holdup value in Eq. (35) depended on the superficial gas velocity ( $U_G$ ) and the flow regime (Chisti, 1989); thus,

$$\varepsilon_G = 2.47U_G^{0.97} \quad (36)$$

for the bubble flow regime ( $U_G < 0.05 \text{ m s}^{-1}$ ), and

$$\varepsilon_G = 0.49U_G^{0.46} \quad (37)$$

for the churn-turbulent flow ( $U_G > 0.05 \text{ m s}^{-1}$ ). Eq. (35) is a purely analytical relationship (Chisti, 1989), whereas Eqs. (34), (36), and (37) were obtained by Chisti (1989) for the same bubble column, fluid, and gas flow rate combinations as discussed in this work. The specific power input for use in Eq. (34) was calculated using the expression:

$$\frac{P_G}{V_L} = \rho_L g U_G \quad (38)$$

Eq. (34) correlated the data to within  $\pm 15\%$ ; the data spanned the ranges:  $1.50 \leq h_L \text{ (m)} \leq 5.875$  and  $6.1 \leq h_L/d_T \leq 24.2$ . Furthermore, Eq. (34) closely agreed with published correlations such as that of Shah et al. (1982) developed for air–water in smaller bubble columns. Similarly, Eqs. (36) and (37) correlated data (air–water) from several sources over the ranges  $0.10 \leq d_T \text{ (m)} \leq 1.067$  and  $h_L$  values up to about 6 m (Chisti, 1989).

The model generated steady-state axial concentration profile and the measured data are shown in Fig. 1. The

modeled curve generally agrees with the data to within  $\pm 3\%$  of the data values. The  $\beta$ -value for the best-fit line in the Fig. was 2.1, which corresponded to an axial dispersion coefficient of  $0.118 \text{ m}^2 \text{ s}^{-1}$ . The straight line in Fig. 1 represents the theoretically calculated dimensionless values of the saturation concentration of dissolved oxygen (Eqs. (2) and (4)) in the absence of any mixing. The data shown in Fig. 1 were for the low-aeration rate – a superficial gas velocity of  $2.70 \times 10^{-2} \text{ m s}^{-1}$  – which corresponded to the bubble flow regime. Similar data are shown in Fig. 2 for the higher gas flow rate of the churn-turbulent regime. Again, the model predicts the behavior to within about  $\pm 3\%$  of the data set. As expected, the best-fit value of the axial dispersion coefficient is now  $0.172 \text{ m}^2 \text{ s}^{-1}$ , or about 45% greater than in the more quiescent environment of bubbly flow. Because the gas holdup (Eqs. (36) and (37)) and the  $k_L a_L$  (Eq. (34)) data used in determining the best-fit  $\beta$  values had been obtained in the same bubble column, a comparison of the model-estimated dispersion coefficients with other published correlations provides an additional test for the model.

A large amount of directly measured data exists on axial dispersion coefficients in bubble columns (Shah et al., 1982; Heijnen and Van't Riet, 1984; Ohki and Inoue, 1970; Deckwer et al., 1974; Joshi, 1980; Baird and Rice, 1975). Generally, dispersion coefficients are not particularly sensitive to the properties of the fluid, the height of the column, or the flow rate of the liquid so long as the latter does not exceed about  $0.1 \text{ m s}^{-1}$ . The axial

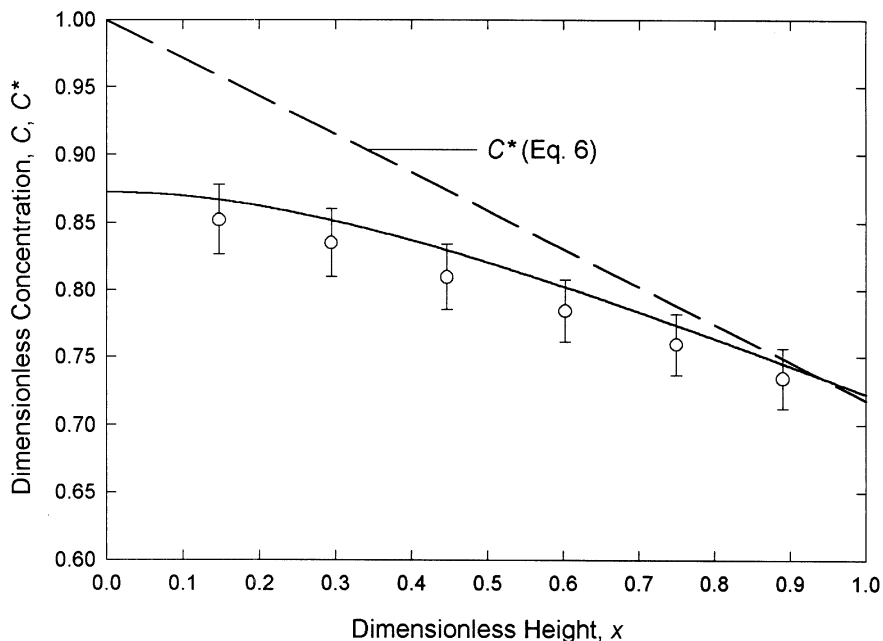


Fig. 1. Dimensionless steady-state dissolved oxygen concentration at various dimensionless axial positions in the bubble column at a superficial gas velocity of  $2.70 \times 10^{-2} \text{ m s}^{-1}$ . The straight line represents the saturation concentration of dissolved oxygen for an axially invariant gas-phase composition. The curve is the model prediction and the measured data are represented as circles with  $\pm 3\%$  error bars. The model parameters were:  $\beta = 2.1$ ,  $k_L a_L = 0.029 \text{ s}^{-1}$ ,  $\varepsilon_G = 0.074$ ,  $D_z = 0.118 \text{ m}^2 \text{ s}^{-1}$ , and  $x_C = 0.95$ .

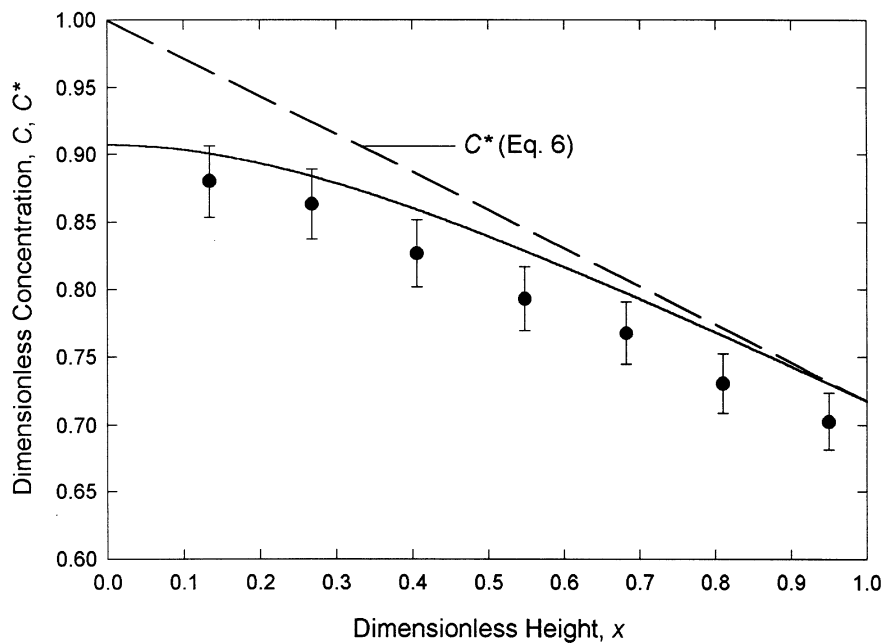


Fig. 2. Dimensionless steady-state dissolved oxygen concentration at various dimensionless axial positions in the bubble column at a superficial gas velocity of  $7.72 \times 10^{-2} \text{ m s}^{-1}$ . The straight line represents the saturation concentration of dissolved oxygen for an axially invariant gas-phase composition. The curve is the model prediction and the measured data are represented as circles. The model parameters were:  $\beta = 3.0$ ,  $k_L a_L = 0.071 \text{ s}^{-1}$ ,  $\varepsilon_G = 0.150$ ,  $D_z = 0.172 \text{ m}^2 \text{ s}^{-1}$ , and  $x_C = 1.0$ .

dispersion coefficients depend only on the diameter ( $d_T$ ) of the bubble column and the superficial gas velocity, or it's equivalent the specific energy input rate. Typically, this dependence has been expressed as follows:

$$D_z = \chi d_T^k U_G^m, \quad (39)$$

where the parameter  $\chi$  is generally less than unity, the  $k$  value exceeds 1.0, and the  $m$  value is usually less than 0.5. In a few instances, the gas sparger hole size and the gas holdup have also been observed to influence the dispersion coefficient (Ohki and Inoue, 1970; Joshi, 1980). For the air–water system that is of interest here, some suitable correlations for  $D_z$  are:

$$D_z = 0.678 d_T^{1.4} U_G^{0.3}, \quad (40)$$

which is due to Deckwer et al. (1974) and

$$D_z = 0.35 d_T^{4/3} E^{1/3}, \quad (41)$$

which is due to Baird and Rice (1975). The correlation propounded by Joshi (1980) also produces dispersion coefficient values that are consistent with those of Eq. (40). In Eq. (41),  $E$  is the energy dissipation rate per unit mass of fluid. In a bubble column,  $E$  depends on the superficial gas velocity as follows:

$$E = g U_G. \quad (42)$$

The dispersion coefficient values calculated using Eqs. (40) and (41) for the two gas flow rates used are shown in Table 1. The table also shows the best-fit dispersion

Table 1  
Comparison of liquid-phase axial dispersion coefficients

Gas velocity $\times 10^2 \text{ (m s}^{-1}\text{)}$	Dispersion coefficient ( $\text{m}^2 \text{ s}^{-1}$ )		
	Eq. (40)	Eq. (41)	Model
2.70	0.032	0.034	0.118
7.72	0.043	0.048	0.172

coefficients obtained by fitting the measured concentration profile with the proposed model. The values given by the model are about 3.5-fold higher than the predictions of experimental correlations. It should be noted that correlations such as Eqs. (40) and (41) predict dispersion coefficients to an accuracy of about  $\pm 50\%$ . Even if this is taken into account, the model-predicted values are high, although dispersion coefficients up to about  $0.12 \text{ m}^2 \text{ s}^{-1}$  have been measured in bubble columns (Reith et al., 1968).

The relatively high values of the model based dispersion coefficients suggest that the shape of the concentration profile is influenced by an additional factor that supplements the axial mixing effect of the liquid-phase. An axially varying  $k_L a_L$  has in the past been used to improve the fit of axial concentration profiles of carbon dioxide in bubble columns with net flow of the liquid phase (Deckwer et al., 1978). Although the overall measured  $k_L a_L$  in bubble columns is independent of the height or the aspect ratio (Chisti, 1989; Shah et al., 1982; Heijnen

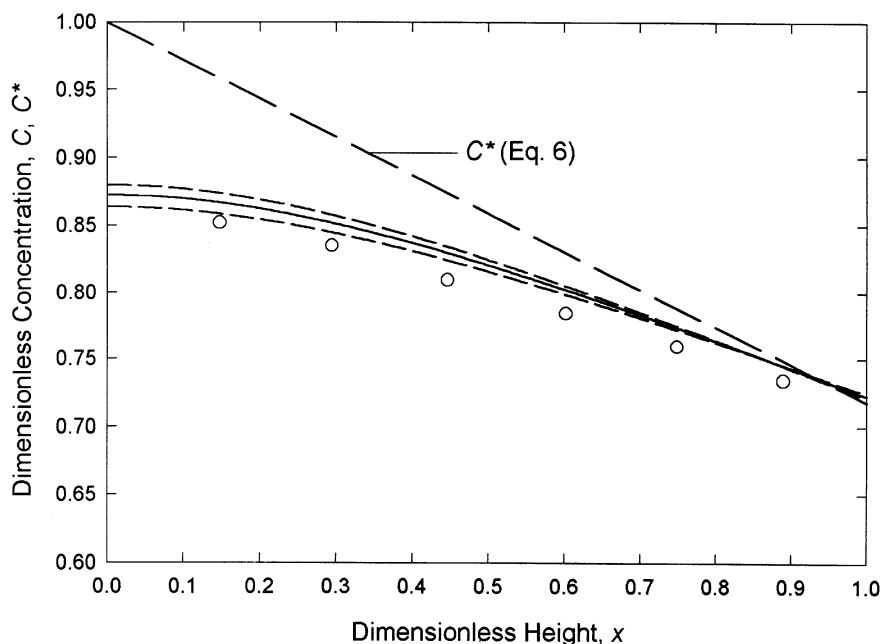


Fig. 3. Dimensionless steady-state dissolved oxygen concentration at various dimensionless axial positions in the bubble column at a superficial gas velocity of  $2.70 \times 10^{-2} \text{ m s}^{-1}$ . The straight line represents the saturation concentration of dissolved oxygen for an axially invariant gas-phase composition. The curve (solid line) is the model prediction for the parameters:  $\beta = 2.1$ ,  $k_L a_L = 0.029 \text{ s}^{-1}$ ,  $\epsilon_G = 0.074$ ,  $D_z = 0.118 \text{ m}^2 \text{ s}^{-1}$ , and  $x_C = 0.95$ . The two dashed curves represent model predictions with  $\pm 15\%$  change in the  $k_L a_L$ .

and Van't Riet, 1984), the local value of  $k_L a_L$  at any axial position varies with height (Deckwer et al., 1978). This is because the gas holdup and the bubble size vary axially (Choi and Lee, 1990; Glasgow et al., 1984; Deckwer et al., 1978), and  $k_L$  is a function of the bubble size (Chisti, 1989; Akita and Yoshida, 1974; Hughmark, 1967; Miller, 1983; Kawagoe et al., 1975) whereas  $a_L$  depends both on the size of the bubble and the gas holdup (Chisti, 1989). The measured overall  $k_L a_L$  is actually a height averaged value; thus,

$$k_L a_L = \frac{1}{h_D} \int_0^{h_D} (k_L a_L)_z dz. \quad (43)$$

Local values of  $k_L a_L$  cannot be measured directly in bubble columns operated batchwise with respect to the liquid phase. Local measurements have never been reported for such columns. Nevertheless, simulations reveal that small variations in the overall  $k_L a_L$  – variations of the order of  $\pm 15\%$  in Eq. (34) – have little impact on the shape or position of the modeled concentration profile as shown in Fig. 3. Consistent with the  $k_L a_L$  data, the overall gas holdup in bubble columns is insensitive to changes in aspect ratio so long as the column diameter exceeds about 0.1 m (Chisti, 1989; Akita and Yoshida, 1973; Fair et al., 1962; Kataoka et al., 1979), yet the local gas holdup in tall bubble columns increases axially up the column (Deckwer et al., 1978; Glasgow et al., 1984).

As a possible additional effect, the steady-state composition of the gas phase may vary axially more than

allowed for in the model which assumes a constant gas phase. Such variations in the gas phase could occur if the small bubble near the bottom of the column reached equilibrium faster with the higher concentration liquid-phase at the bottom, moved up the column with the fluid streams, and transferred some of the gas to the liquid phase higher up. This effect could reduce non-uniformity in the axial liquid-phase concentrations and it would give rise to a high apparent liquid-phase axial dispersion coefficient. What is clearly obvious, is that liquid-phase axial dispersion alone cannot explain the axial concentration profiles if a constant gas-phase composition is assumed. To resolve the issue of high estimated values of the axial dispersion coefficients, the gas-phase composition was allowed to vary in a set of model simulations. Thus, instead of Eq. (6), the dimensionless saturation concentration ( $C^*$ ) varied according to the polynomial

$$C^* = a + b(1 - x) + j(1 - x)^2, \quad (44)$$

where  $a$ ,  $b$ , and  $j$  are constants. Of these constants,  $a$  is equivalent to  $\psi$  of Eq. (6), but  $b$  and  $j$  are entirely arbitrary. The parameters  $b$ ,  $j$ , and  $\beta$  were varied to obtain a best-fit between the measured concentration profile and the calculated profile (Eq. 33). As an additional constraint, the  $C^*$  value at  $x = 0$  and  $x = 1$  had to be identical to those computed with Eq. (6), i.e., the mole fraction of oxygen in the inlet and outlet air was 0.21. Again, the  $k_L a_L$  and  $h_D$  values in the best-fit  $\beta$  had to agree with Eqs. (34) and (35). Following this approach, the fit of the modeled axial concentration profile and

the measured data improved greatly as illustrated in Fig. 4 which is for the same measurements as Fig. 1. Furthermore, the best-fit value of the axial dispersion coefficient was  $0.041 \text{ m}^2 \text{ s}^{-1}$ , or within 20% of that computed with the empirical Eq. (41). The  $a$ ,  $b$ , and  $j$  values were 0.72, 0.006, and 0.28, respectively. The gas-phase mole fraction of oxygen varied axially as shown in Fig. 5. The maximum variation from the inlet or the outlet composition was less than 10%. The profile in Fig. 5 was computed with the equation

$$y_{O_2}|_x = \frac{a + b(1-x) + j(1-x)^2}{\left(\frac{\psi}{0.21}\right) + \left(\frac{\alpha}{0.21}\right)(1-x)} \quad (45)$$

As shown in Fig. 4, the mass transfer reversal location  $x_c$  now occurred about half-way up the column, suggesting that the end-effect of the liquid surface was negligible. Similar results were obtained for the data shown in Fig. 2 when the gas-phase oxygen composition was allowed to vary. Now, the best-fit parameter values were:  $a = 0.72$ ,  $b = 0.11$ ,  $j = 0.16$ ,  $\beta = 5.4$ , and  $D_z = 0.055 \text{ m}^2 \text{ s}^{-1}$ . The latter was within 15% of predictions of Eq. (41). Although a non-constant gas-phase composition improves the fit of the modeled profile with the measurements and the value of the axial dispersion coefficient becomes consistent with independent measurements, additional parameters  $b$  and  $j$  are introduced and the  $C^*$  Eq. (44) loses physical sense. In view of these shortcomings and the small change ( $< 10\%$ ) in the gas-phase

composition, the analysis based on a constant gas-phase concentration of oxygen (i.e., Eq. (6)) remains a good approximation.

Another aspect that is of interest is the sensitivity of the steady-state dissolved oxygen profile to variation in the gas flow rate, the gas holdup, the  $k_L a_L$ , and the axial liquid-phase dispersion coefficient. Chisti (1989) experimentally showed that the concentration profiles did not vary significantly with changes in gas flow rate within values typically used in bubble columns. Consequently, small variations in gas holdup, the  $k_L a_L$ , and the axial liquid-phase dispersion coefficient – all of which are influenced mainly by the gas flow rate – should not affect the shape of the concentration profiles. The model based simulations shown in Figs. 3, 6 and 7 confirm this point. Thus, the concentration profile is little affected by  $\pm 20$  and  $\pm 40\%$  variation in  $D_z$  around the best-fit  $D_z$  values (Fig. 6), and by  $\pm 15\%$  variation in the gas holdup (Fig. 7) around the values calculated with Eq. (36). Note that those levels of variations represent extremes; for example, a variation of  $\pm 10\%$  is more realistic for gas holdup.

A lack of substantial influence of the gas flow rate on the shape of the profile is clearly explained by the model: the parameter  $\beta$  is not too sensitive to gas flow velocity because the  $k_L a_L$  and the axial dispersion coefficient – both of which increase with increasing gas flow rate – influence  $\beta$  in opposing ways. From the known relationships between superficial gas velocity,  $k_L a_L$  (Eqs. (34) and (38)), and the axial dispersion coefficient (Eq. (40)), the parameter  $\beta$  can be shown to follow the approximate

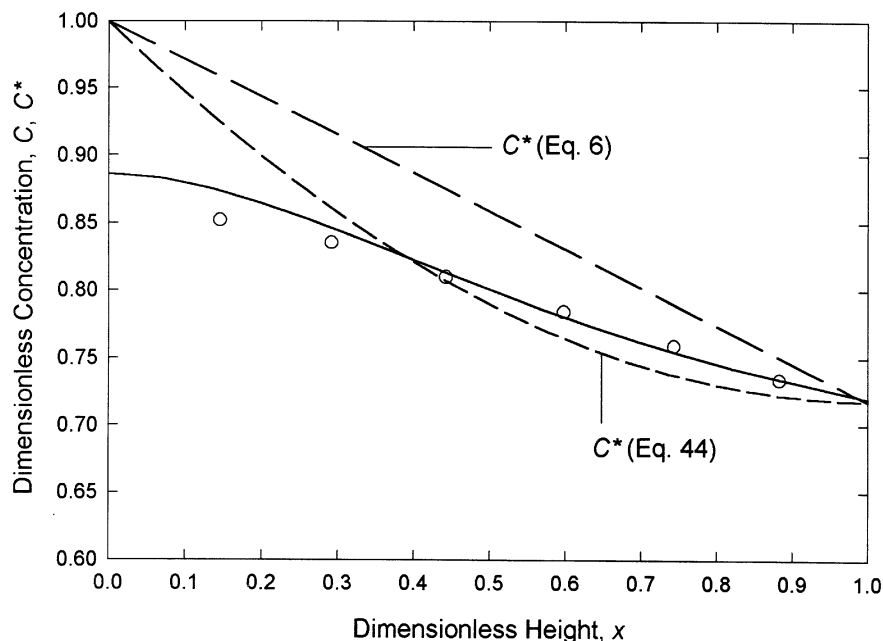


Fig. 4. Dimensionless steady-state dissolved oxygen concentration at various dimensionless axial positions in the bubble column at a superficial gas velocity of  $2.70 \times 10^{-2} \text{ m s}^{-1}$ . A non-constant gas-phase composition (Eq. (44)) was used. The straight line represents Eq. (6). The modeled profile agrees with the data closely. The model parameters were:  $\beta = 3.6$ ,  $k_L a_L = 0.029 \text{ s}^{-1}$ ,  $\epsilon_G = 0.074$ ,  $D_z = 0.041 \text{ m}^2 \text{ s}^{-1}$ ,  $a = 0.72$ ,  $b = 0.006$ , and  $j = 0.28$ .

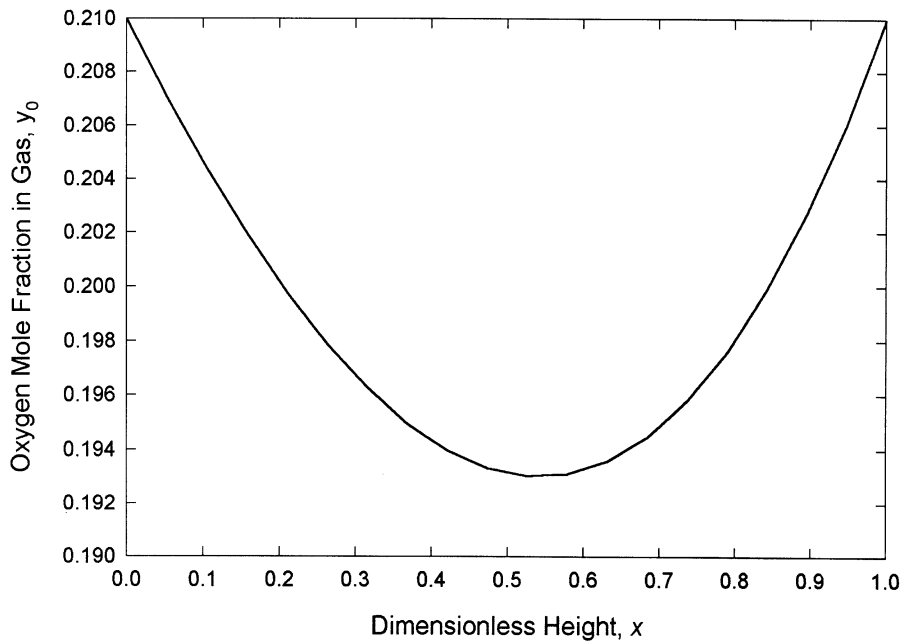


Fig. 5. The oxygen mole fraction in the gas phase as a function of the dimensionless axial position in the bubble column at a superficial gas velocity of  $2.70 \times 10^{-2} \text{ m s}^{-1}$ . The profile was calculated using Eq. (45) with  $\psi = a = 0.72$ ,  $b = 0.006$ , and  $j = 0.28$ .

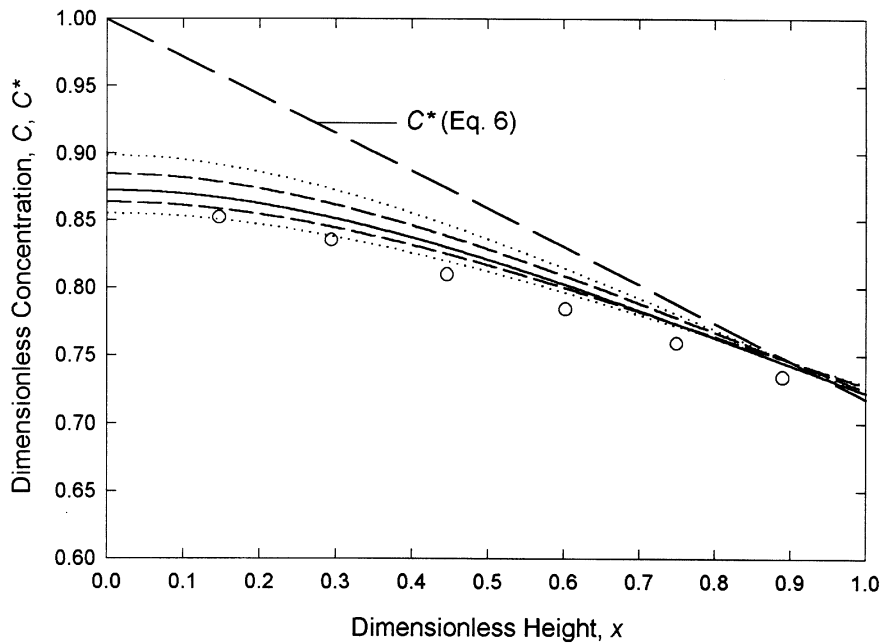


Fig. 6. Dimensionless steady-state dissolved oxygen concentration at various dimensionless axial positions in the bubble column at a superficial gas velocity of  $2.70 \times 10^{-2} \text{ m s}^{-1}$ . The straight line represents the saturation concentration of dissolved oxygen for an axially invariant gas-phase composition. The curve (solid line) is the model prediction for the parameters:  $\beta = 2.1$ ,  $k_L a_L = 0.029 \text{ s}^{-1}$ ,  $\epsilon_G = 0.074$ ,  $D_z = 0.118 \text{ m}^2 \text{ s}^{-1}$ , and  $x_C = 0.95$ . The four dashed curves represent model predictions with  $\pm 20$  and  $\pm 40\%$  changes in  $D_z$ .

relationship  $\beta x U_G^{0.28}$  which is a relatively weak dependence on the gas flow rate.

The measurements discussed here were obtained in a column that was 3.995 m tall. How will further increases

in height affect the shape of the concentration profiles? This question is answered by the simulation shown in Fig. 8 where the profiles are shown for dispersion heights  $h_D$  of 2.2, 4.3, and 6.5 m in a 0.243 m diameter column. Clearly,

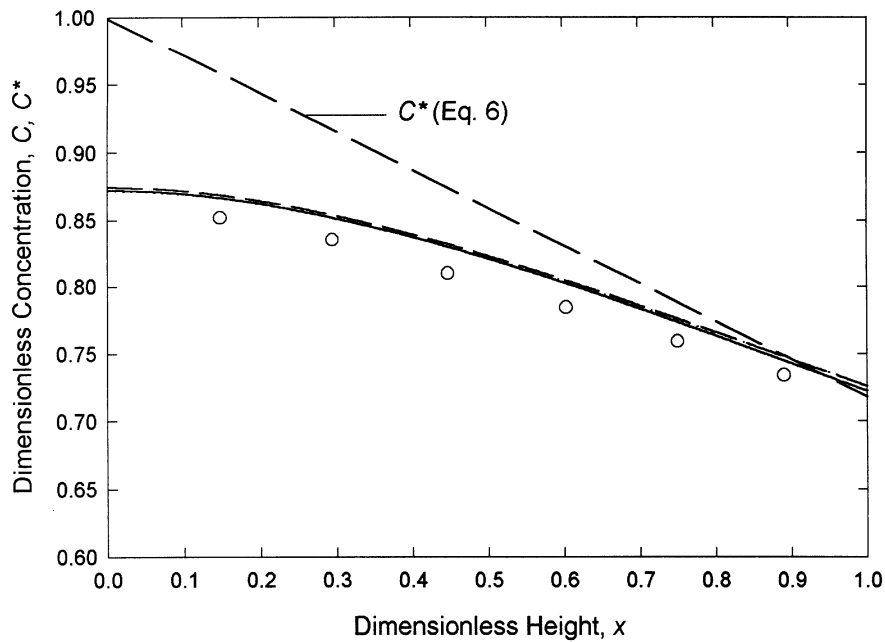


Fig. 7. Dimensionless steady-state dissolved oxygen concentration at various dimensionless axial positions in the bubble column at a superficial gas velocity of  $2.70 \times 10^{-2} \text{ m s}^{-1}$ . The straight line represents the saturation concentration of dissolved oxygen for an axially invariant gas-phase composition. The curve (solid line) is the model prediction for the parameters:  $\beta = 2.1$ ,  $k_L a_L = 0.029 \text{ s}^{-1}$ ,  $\varepsilon_G = 0.074$ ,  $D_z = 0.118 \text{ m}^2 \text{ s}^{-1}$ , and  $x_C = 0.95$ . The two dashed curves represent model predictions with  $\pm 15\%$  change in gas holdup.

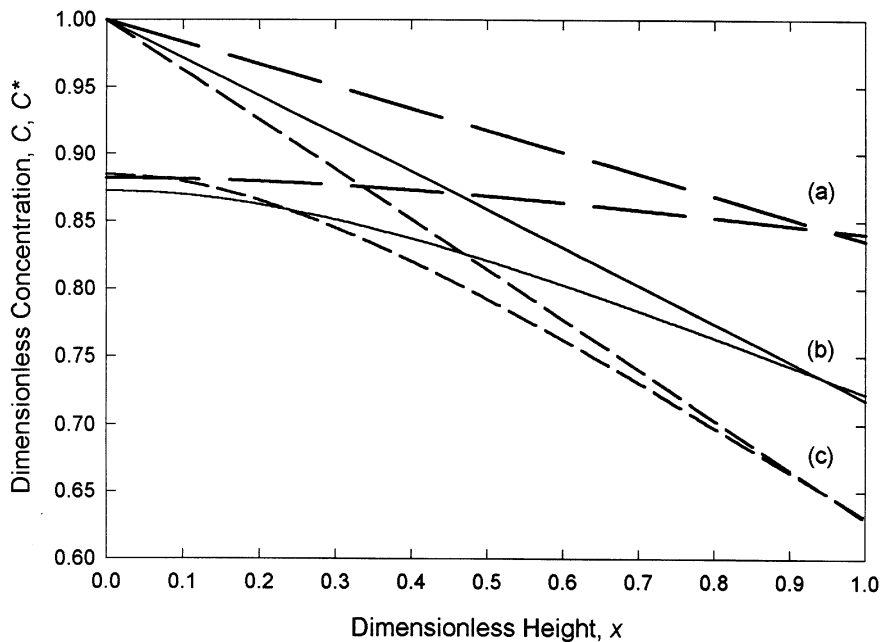


Fig. 8. Dimensionless steady-state dissolved oxygen concentration at various dimensionless axial positions in the bubble column at a superficial gas velocity of  $2.70 \times 10^{-2} \text{ m s}^{-1}$ . The straight line represents the saturation concentration of dissolved oxygen for an axially invariant gas-phase composition and overall dispersion heights of (a) 2.2 m; (b) 4.3 m; and (c) 6.5 m. The middle curve is the model prediction for the parameters:  $\beta = 2.1$ ,  $k_L a_L = 0.029 \text{ s}^{-1}$ ,  $\varepsilon_G = 0.074$ ,  $D_z = 0.118 \text{ m}^2 \text{ s}^{-1}$ ,  $x_C = 0.95$ , and overall dispersion height,  $h_D = 4.3 \text{ m}$ . The other two curves are model predictions for  $h_D = 6.5 \text{ m}$  (lower), and  $h_D = 2.2 \text{ m}$  (upper), with the other parameters remaining unchanged.

in relatively short columns – up to 2.2 m tall (aspect ratio  $\approx 9$ ) – the axial variation in concentration is barely detectable; however, the axial variation becomes more pronounced as the height of column increases.

The strong dependence of the axial dispersion coefficient on diameter of bubble column suggests that for a given superficial gas velocity and height of static liquid, the axial steady-state dissolved oxygen profile should

depend on the aspect ratio of a column. This must be so because the other two relevant parameters – the overall gas holdup and the  $k_L a_L$  – are known to be independent of aspect ratio so long as the column diameter exceeds about 0.1 m (Chisti, 1989; Akita and Yoshida, 1973; Fair et al., 1962; Kataoka et al., 1979). Although in the past the axial dispersion coefficient has been observed to depend strongly on the diameter of the column, this dependence has not been adequately explained. One possible explanation follows: Even in a column with no net flow of liquid, there is a distinct pattern of liquid circulation. The radial liquid velocity profile has been measured (Ueyama and Miyauchi, 1979). The liquid flows up the center of the column and a net downflow exists in an annular region next to the walls. Increasing axial dispersion coefficient with increasing column diameter implies an increase in the velocity of liquid circulation for otherwise unchanged conditions. This increase in circulation could occur if the frictional resistance to circulation were to decline. The latter should happen because the hydraulic diameter for an arbitrary annular downflow zone – the zone next to the walls where the frictional resistance is greatest – can be shown to increase with increasing diameter of the column: The column can be imagined as consisting of an arbitrary central upflow zone with a cross-sectional area  $A_r$ ; similarly, the downflow annular zone has an arbitrary cross-sectional area  $A_d$ . Based on the observations of Ueyama and Miyauchi (1979), the location of the flow inversion boundary – i.e., the boundary between the upflow and downflow zones – is insensitive to the diameter of the column. This point has been demonstrated for a diameter range of 0.25–0.6 m (Ueyama and Miyauchi, 1979); therefore, the  $A_r/A_d$  ratio does not depend on the column diameter, i.e.,

$$\frac{A_r}{A_d} = c, \quad (46)$$

where  $c$  is a constant. Also, from geometric reasoning

$$A_r + A_d = \frac{\pi d_T^2}{4}, \quad (47)$$

where  $d_T$  is the diameter of the column. Now, because the hydraulic diameter  $d_h$  of the annular downflow zone is given by

$$d_h = \frac{4 \times \text{flow area}}{\text{wetted perimeter}} = \frac{4A_d}{\pi d_T}, \quad (48)$$

from Eqs. (46)–(48), we have

$$d_h = \frac{d_T}{c + 1}. \quad (49)$$

Thus,  $d_h$  increases with increasing  $d_T$ ; hence, resistance to liquid circulation declines, and  $D_z$  increases. In fact, the increase in  $D_z$  is stronger than can be explained solely by the change in the frictional resistance to flow, which

implies enhanced mixing between the upflowing and the downflowing liquid streams all along the height of the column. This enhancement in mixing should increase with increasing superficial velocities of the streams.

Existence of a radial liquid velocity profile suggests a radial variation in the local gas holdup. Such variations – higher holdup in the central core and lower values in the periphery – have indeed been observed (Lippert et al., 1983). Although in a bubble column there is no separating wall or draft-tube between the upflow and the downflow zones as exists in an airlift reactor, it is conceivable that the rate of liquid circulation increases in proportion to the square root of the height of dispersion as happens in airlift reactors (Chisti, 1989, 1998). It is, therefore, likely that columns with exceptionally large aspect ratios will have higher values of liquid-phase dispersion coefficients than given by Eqs. (40) and (41). It is noteworthy that the aspect ratio used in this study was relatively high at  $\sim 16.5$ . Although Deckwer et al. (1978) previously employed columns with aspect ratios of 29 and 36, the measurements were made in flow-through modes; hence, the characteristic upflow/downflow pattern of batch bubble columns could not have existed.

## 5. Conclusions

The steady-state concentration of dissolved oxygen varies axially in a bubble column. The axial concentration profile is flatter than expected from application of Henry's law to an unmixed column. The measured concentration profile is closely correlated by a model that employs a liquid-phase axial dispersion coefficient as a fitting parameter. The shape of the axial concentration profile is influenced by the overall gas holdup, the overall volumetric gas–liquid mass transfer coefficient, and the axial dispersion coefficient, all of which are affected by the gas flow rate. The static height of liquid in the column also affects the concentration profile. Because the  $k_L a_L$  and the dispersion coefficient have opposing effects on the axial concentration profile, the profile is not exceedingly sensitive to the superficial gas velocity; however, the profile become flatter with increasing gas flow rate. The proposed model provides an elegant tracer-less method for determining the axial dispersion coefficient value in an operating bubble column bioreactor using the easily measured axial concentration profile. The measurement need not interrupt the operation of the reactor in any way. The model-estimated axial dispersion coefficient values are consistent with independent measurements when a non-constant gas-phase composition is allowed. Alternatively, the model can be used to predict spatial variations in dissolved oxygen concentration in tall bubble columns if suitable correlations are available for calculating the axial dispersion coefficient, the  $k_L a_L$ , and the gas holdup. Based on the model, in the absence of

consumption, the steady-state oxygen concentration in the gas-phase varies axially by up to 10% in a column that is about 4 m tall. Oxygen is transferred from the gas to the liquid-phase in the lower half of the column, but reverse transfer occurs in the upper region. The theoretical saturation concentration cannot be achieved at all axial locations in a tall bubble column even in the absence of an oxygen consuming reaction unless air is injected at multiple locations spaced along the height of the column.

## Notation

$a$	parameter in Eqs. (44) and (45), dimensionless
$a_L$	gas–liquid interfacial area per unit liquid volume, $\text{m}^{-1}$
$A_d$	cross-sectional area of annular downflow zone, $\text{m}^2$
$A_L$	area of the liquid surface, $\text{m}^2$
$A_r$	cross-sectional area of central upflow zone, $\text{m}^2$
$b$	parameter in Eqs. (44) and (45), dimensionless
$c$	dimensionless constant defined by Eq. (46)
$\text{cte}_1$	constant of integration, dimensionless
$\text{cte}_2$	constant of integration, dimensionless
$C$	dimensionless concentration, dimensionless
$C_0$	actual concentration of dissolved oxygen, $\text{kg m}^{-3}$
$C^*$	dimensionless saturation concentration of dissolved oxygen, $\text{kg m}^{-3}$
$C_0^*$	saturation concentration of dissolved oxygen, $\text{kg m}^{-3}$
$d_h$	hydraulic diameter of the annular downflow zone, m
$d_T$	diameter of column, m
$D_z$	overall axial dispersion coefficient of liquid, $\text{m}^2 \text{s}^{-1}$
$E$	energy dissipation rate per unit mass, $\text{W kg}^{-1}$
$g$	gravitational acceleration, $\text{m s}^{-2}$
$h_D$	height of dispersion, m
$h_L$	height of gas-free liquid, m
$H_0$	Henry's law constant, $\text{Pa kg}^{-1} \text{m}^3$
$j$	parameter in Eqs. (44) and (45), dimensionless
$k$	exponent in Eq. (39), dimensionless
$k_L$	liquid film mass transfer coefficient, $\text{m s}^{-1}$
$k_{LA}$	overall gas–liquid volumetric mass transfer coefficient, $\text{s}^{-1}$
$m$	exponent in Eq. (39), dimensionless
$P_a$	pressure in the headspace of the column, Pa
$P_b$	hydrostatic pressure at the bottom of the column, Pa
$P_G$	power input due to gas, W
$P(z)$	hydrostatic pressure at height $z$ from the bottom, Pa
$R$	overall rate of reaction, $\text{kg m}^{-3} \text{s}^{-1}$
$S$	cross-sectional area of the column, $\text{m}^2$

$U_G$	superficial gas velocity, $\text{m s}^{-1}$
$V_L$	volume of liquid, $\text{m}^3$
$x$	dimensionless axial height
$x_C$	dimensionless axial position at which the direction of mass transfer reverses
$y_0$	mole fraction of oxygen in the gas phase, dimensionless
$z$	axial distance, m

## Greek letters

$\alpha$	dimensionless parameter defined by Eq. (7)
$\beta$	dimensionless parameter defined by Eq. (9)
$\varepsilon_G$	overall gas holdup, dimensionless
$\pi$	Pi, dimensionless
$\rho_L$	density of the liquid, $\text{kg m}^{-3}$
$\phi$	dimensionless parameter defined by Eq. (30)
$\chi$	parameter in Eq. (39), $\text{m}^{2-(k+m)} \text{s}^{m-1}$
$\psi$	dimensionless parameter defined by Eq. (8)

## References

- Akita, K., & Yoshida, F. (1973). Gas holdup and volumetric mass transfer coefficient in bubble columns. *Ind. Engng Chem. Process Des. Dev.*, 12, 76–80.
- Akita, K., & Yoshida, F. (1974). Bubble size, interfacial area, and liquid-phase mass transfer coefficient in bubble columns. *Ind. Engng Chem. Process Des. Dev.*, 13, 84–91.
- Baird, M.H.I., & Rice, R. G. (1975). Axial dispersion in large unbaffled columns. *Chem. Engng J.*, 9, 171–174.
- Chisti, Y. (1989). *Airlift Bioreactors* (pp. 355). London: Elsevier.
- Chisti, Y. (1998). Pneumatically agitated bioreactors in industrial and environmental bioprocessing: Hydrodynamics, hydraulics and transport phenomena. *Appl. Mech. Rev.*, 51, 33–112.
- Choi, K.H., & Lee, W.K. (1990). Comparison of probe methods for measurement of bubble properties. *Chem. Engng Commun.*, 91, 35–47.
- Deckwer, W.-D., Adler, I., & Zaidi, A. (1978). A comprehensive study on  $\text{CO}_2$ -interphase mass transfer in vertical cocurrent and countercurrent gas–liquid flow. *Can. J. Chem. Engng*, 56, 43–55.
- Deckwer, W.-D., Burkhart, R., & Zoll, G. (1974). Mixing and mass transfer in tall bubble columns. *Chem. Engng Sci.*, 29, 2177–2188.
- Fair, J.R., Lambright, A.J., & Andersen, J.W. (1962). Heat transfer and gas holdup in a sparged contactor. *Ind. Engng Chem. Process Des. Dev.*, 1, 33–36.
- Glasgow, L.A., Erickson, L.E., Lee, C.H., & Patel, S.A. (1984). Wall pressure fluctuations and bubble size distributions at several positions in an airlift fermentor. *Chem. Engng Commun.*, 29, 311–336.
- Heijnen, J.J., & Van't Riet, K. (1984). Mass transfer, mixing and heat transfer phenomena in low viscosity bubble column reactors. *Chem. Engng J.*, 28, B21–B42.
- Hughmark, G.A. (1967). Holdup and mass transfer in bubble column. *Ind. Engng Chem. Process Des. Dev.*, 6, 218–220.
- Joshi, J.B. (1980). Axial mixing in multiphase contactors – A unified correlation. *Trans. Instn Chem. Engrs*, 58, 155–165.
- Kataoka, H., Takeuchi, H., Nakao, H., Yagi, H., Tadaki, T., Otake, T., Miyauchi, T., Washimi, K., Watanabe, K., & Yoshida, F. (1979). Mass transfer in a large bubble column. *J. Chem. Engng Jpn*, 12, 105–110.
- Kawagoe, M., Nakao, H., & Otake, T. (1975). Liquid-phase mass transfer coefficient and bubble size in gas sparged contactors. *J. Chem. Engng Jpn*, 8, 254–256.

- Krebs, W.M., & Haddad, I.A. (1972). The oxygen electrode in fermentation systems. *Dev. Ind. Microbiol.*, 13, 113–127.
- Lippert, J., Adler, I., Meyer, H.D., Lübbert, A., & Schügerl, K. (1983). Characterization of the two-phase systems in airlift tower-loop bioreactors during the cultivation of *E. coli*. *Biotechnol. Bioengng*, 25, 437–450.
- Miller, D.N. (1983). Interfacial area, bubble coalescence and mass transfer in bubble column reactors. *A.I.Ch.E. J.*, 29, 312–319.
- Ohki, Y., & Inoue, H. (1970). Longitudinal mixing of the liquid phase in bubble columns. *Chem. Engng Sci.*, 25, 1–16.
- Pollard, D.J., Ison, A.P., Ayazi Shamlou, P., & Lilly, M.D. (1994). The examination of bioreactor heterogeneity with rheological different fermentation broths. In E. Galindo, & O.T. Ramirez, (Eds.) *Advances in Bioprocess Engineering* (pp. 163–170). Dordrecht: Kluwer.
- Reith, T., Renken, S., & Israël, B.A. (1968). Gas hold-up and axial mixing in the fluid phase of bubble columns. *Chem. Engng Sci.*, 23, 619–629.
- Russell, A.B., Thomas, C.R., & Lilly, M.D. (1995). Oxygen transfer measurements during yeast fermentations in a pilot scale airlift fermenter. *Bioproc. Engng*, 12, 71–79.
- Shah, Y.T., Kelkar, B.G., Godbole, S.P., & Deckwer, W.-D. (1982). Design parameters estimations for bubble column reactors. *A.I.Ch.E. J.*, 28, 353–379.
- Ueyama, R., & Miyauchi, T. (1979). Properties of recirculating turbulent two phase flow in gas bubble columns. *A.I.Ch.E. J.*, 25, 258–266.